

LETTER TO THE EDITOR

The first Herschel view of the mass-SFR link in high- z galaxies [★]

G. Rodighiero¹, A. Cimatti², C. Gruppioni³, P. Popesso⁴, P. Andreani^{5,13}, B. Altieri⁷, H. Aussel⁸, S. Berta⁴, A. Bongiovanni⁹, D. Brisbin¹⁰, A. Cava⁹, J. Cepa⁹, E. Daddi⁸, H. Dominguez-Sanchez³, D. Elbaz⁸, A. Fontana⁶, N. Förster Schreiber⁴, A. Franceschini¹, R. Genzel⁴, A. Grazian⁶, D. Lutz⁴, G. Magdis⁸, M. Magliocchetti¹¹, B. Magnelli⁴, R. Maiolino⁶, C. Mancini¹², R. Nordon⁴, A. M. Perez Garcia, A. Poglitsch⁴, P. Santini⁶, M. Sanchez-Portal⁷, F. Pozzi², L. Riguccini⁸, A. Saintonge⁴, L. Shao⁴, E. Sturm⁴, L. Tacconi⁴, I. Valtchanov⁷, M. Wetzstein⁴, and E. Wierucht⁴

(See online Appendix A for author affiliations)

Received March 31, 2010 accepted

ABSTRACT

Aims. We exploit deep observations of the GOODS-N field taken with PACS, the *Photodetector Array Camera and Spectrometer*, on board of *Herschel*, as part of the *PACS Evolutionary Probe* guaranteed time (PEP), to study the link between star formation and stellar mass in galaxies to $z \sim 2$.

Methods. Starting from a stellar mass – selected sample of ~ 4500 galaxies with $\text{mag}_{4.5\mu\text{m}} < 23.0$ (AB), we identify ~ 350 objects with a PACS detection at 100 or 160 μm and ~ 1500 with only *Spitzer* 24 μm counterpart. Stellar masses and total IR luminosities (L_{IR}) are estimated by fitting the Spectral Energy Distributions (SEDs).

Results. Consistently with other *Herschel* results, we find that L_{IR} based only on 24 μm data is overestimated by a median factor ~ 1.8 at $z \sim 2$, whereas it is underestimated (with our approach) up to a factor ~ 1.6 at $0.5 < z < 1.0$. We then exploit this calibration to correct L_{IR} based on the MIPS/*Spitzer* fluxes. These results clearly show how *Herschel* is fundamental to constrain L_{IR} , and hence the SFR, of high redshift galaxies. Using the galaxies detected with PACS (and/or MIPS), we investigate the existence and evolution of the relations between the star formation rate (SFR), the specific star formation rate (SSFR=SFR/mass) and the stellar mass. Moreover, in order to avoid selection effects, we also repeat this study through a stacking analysis on the PACS images to fully exploit the far-IR information also for the *Herschel* and *Spitzer* undetected subsamples. We find that the SSFR-mass relation steepens with redshift, being almost flat at $z < 1.0$ and reaching a slope of $\alpha = -0.50_{-0.16}^{+0.13}$ at $z \sim 2$, at odds with recent works based on radio-stacking analysis at the same redshift. The mean SSFR of galaxies increases with redshift, by a factor ~ 15 for massive $M > 10^{11} M_{\odot}$ galaxies from $z = 0$ to $z = 2$, and seems to flatten at $z > 1.5$ in this mass range. Moreover, the most massive galaxies have the lowest SSFR at any z , implying that they have formed their stars earlier and more rapidly than their low mass counterparts (*downsizing*).

Key words. Galaxies: evolution – Galaxies: active – Galaxies: starburst – Cosmology: observations – Infrared: galaxies

1. Introduction

The link between galaxy stellar mass and star formation rate (SFR), and its cosmic evolution is crucial to shed light on the processes of galaxy formation. The specific SFR (SSFR = SFR/mass) plays an important role as it measures the star formation efficiency of a galaxy and the fraction of a galaxy mass can be converted into stars per unit time (see e.g. de Cunha et al. 2010). Several studies at $0 < z < 3$ report similar findings: (1) the SSFR increases with redshift at all masses; (2) the SSFR of massive galaxies is lower at all z (e.g. Feulner et al. 2005, Erb et al. 2006, Perez-Gonzalez et al. 2008, Damen et al. 2009, Dunne et al. 2009). However, the scatter and the exact slopes of these relations are still not clear. In particular, the dependence of SSFR on mass is one of the most debated open questions. On the one hand, radio-stacking analysis of galaxies at $z = 1.5 - 2.0$ selected in the K -band found a weak (or even absent) SSFR-mass correlation, with an indication of steepening at higher redshift (Pannella et al. 2009, Dunne et al. 2009). On the other hand, other results based on UV to mid-IR SFR tracers indicate a clear decrease of the SSFR with increasing mass (e.g. Feulner et al. 2005, Erb et al. 2006, Noeske et al. 2007b, Cowie & Barger 2008). Some of

these discrepancies could be due on one hand to the effects of dust extinction corrections for the SFR estimates based on UV-optical indicators, and on the other hand to the assumptions and large extrapolations on the infrared SED shape and luminosity adopted for the SFR estimates based on 24 μm data.

The advent of the *Herschel Space Observatory* (Pilbratt et al. (2010) finally allows us to robustly derive the total infrared (IR) luminosity (L_{IR}) of galaxies, by directly sampling the peak of the thermal emission of dusty galaxies up to $z \sim 3$. In order to place new and stringent constraints on the SSFR evolution, in this work we exploit the PACS Evolutionary Probe (PEP) guaranteed time data collected in the GOODS-North field with the PACS (Poglitsch et al. 2010) instrument. The PEP observations are described in Berta et al. (2010, this Issue Appendix A). Ancillary data, both photometric and spectroscopic, including UV (GALEX), optical (HST), near-IR (FLAMINGOS, IRAC/*Spitzer*) and mid-IR (MIPS/*Spitzer*) data, have been collected to build up a reliable multiwavelength catalog and photometric redshifts. We adopt $h = 0.7$, $\Omega_{\Lambda} = 0.73$ and $\Omega_m = 0.27$.

2. Sample selection

Our aim is to investigate the evolutionary link between stellar mass and star formation avoiding strong biases and selection effects. Thus, the main galaxy sample was selected at 4.5 μm

[★] Herschel is an ESA space observatory with science instruments provided by European-led Principal Investigator consortia and with important participation from NASA.

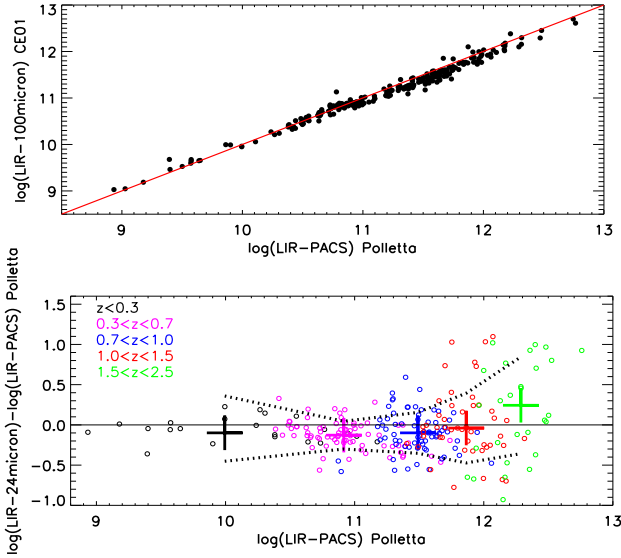


Fig. 1. *Top panel:* Comparison of L_{IR} derived from the UV-to-PACS $24\mu\text{m}$ data with the Polletta templates and the Chary & Elbaz (2001) libraries, by fitting one single point ($100\mu\text{m}$). *Bottom panel:* Comparison of L_{IR} derived from the UV-to- $24\mu\text{m}$ and the UV-to-PACS SED fitting procedures. Different colors refer to various redshift intervals (see legend in the figure). The thick cross symbols represent the median value in the corresponding luminosity bins. We also report with dotted lines the $\pm 1\sigma$ limits around the median. In both panels only sources from the $4.5\mu\text{m}$ catalog that were detected with $\text{SNR} > 3$ at all 24 , 100 and/or $160\mu\text{m}$ are reported.

with IRAC ($\text{mag}_{4.5\mu\text{m}} < 23.0$, AB) in order to ensure sensitivity to stellar mass up to $z \sim 2 - 3$. At this limiting magnitude, the IRAC sample is $\sim 80\%$ flux complete (Mancini et al. 2009), it is not strongly affected by confusion (see Rodighiero et al. 2010) and it includes 4459 sources. On the IRAC positions we fitted PSFs to the MIPS and PACS images (however, for detections in the PACS maps we used only IRAC positions with a $24\mu\text{m}$ detection). Out of the 4459 IRAC sources, 1887 (351) sources have MIPS (PACS) fluxes with signal-to-noise ratio (SNR) greater than 3. The typical $24\mu\text{m}$, $100\mu\text{m}$ and $160\mu\text{m}$ fluxes in this catalog reach the $3\text{-}\sigma$ limit, that is $\sim 20\mu\text{Jy}$ (Magnelli et al. 2009), $\sim 3\text{mJy}$ and $\sim 5.7\text{mJy}$, respectively. With this selection we miss only 2 PACS-detected objects with low signal-to-noise ratio ($\text{SNR} \sim 3$). About 40%, $\sim 52\%$ and $\sim 70\%$ of the IRAC, MIPS and PACS subsamples have an optical spectroscopic redshift (mainly from Barger et al. 2008), respectively.

3. Stellar masses and IR luminosities

Following the approach of Rodighiero et al. (2007), stellar masses were estimated by setting the redshift (photometric or spectroscopic) of each IRAC-selected object and using the *Hyperz* code (Bolzonella et al. 2000) applied to the photometric SEDs in the optical-to- $5.8\mu\text{m}$ range. For an easier comparison with literature data, we used the stellar-population synthesis models of Bruzual & Charlot (2003, hereafter BC03) with a Salpeter IMF, exponentially declining τ models for the SFR, and solar metallicity. We estimated the stellar mass completeness as a function of redshift as described in Mancini et al. (2009) (see online Figure B.1).

For the objects detected with PACS and MIPS, the IR luminosities L_{IR} were estimated with a best fitting procedure by comparing the optical-to-IR SEDs with a library of template SEDs of local objects from Polletta et al. (2007) and adding a few modified templates (see Gruppioni et al. 2010). We followed the same approach that we applied to $24\mu\text{m}$ GOODS-South and SWIRE-VVDS sources in Rodighiero et al. (2010) and in Gruppioni et al. (2010). The inclusion of the whole SED in the fitting procedure allowed us to fully exploit the photometric information and determine the K-correction in the most reliable way. As described in Rodighiero et al. (2010), we forced the spectral fit to reproduce the far-IR *Spitzer-Herschel* datapoints by reducing their photometric errors. To minimize the contribution from AGN emission to the L_{IR} , we removed from our sample X-ray detected sources with $L_X > 10^{42}$ erg/s and those objects classified by the SED fitting analysis as Type 1 quasars. A few examples of our best-fits are presented in the online Appendix C, Figure C.1.

4. The estimate of SFR

For the galaxies detected with PACS or at $24\mu\text{m}$, the instantaneous SFR was estimated using the combination of IR and UV luminosity as in Papovich et al. (2007) and Santini et al. (2009): $SFR_{IR+UV}/M_\odot\text{yr}^{-1} = 1.8 \times 10^{-10} \times L_{bol}/L_\odot$ with $L_{bol} = 2.2 \times L_{UV} + L_{IR}$, where L_{IR} was derived by integrating the best-fit SEDs in the $[8\text{-}1000]\mu\text{m}$ rest-frame range. The rest-frame UV luminosity (which accounts for the contribution for young unobscured stars), uncorrected for extinction, derived from the SED fitting with BC03 model, is $L_{UV} = 1.5 \times L(2700\text{\AA})$. The contribution from L_{UV} is marginal, and its exclusion does not change the results presented here. In the rest of the paper, we will then discuss the main evolutionary trends linking mass and SFR by considering only $\lambda \geq 24\mu\text{m}$ detections, and we will discuss the contribution of the remaining far-IR undetected IRAC sources through a stacking analysis.

5. Results

5.1. Spitzer vs Herschel IR luminosities

The reliability of our IR luminosities was assessed by comparing them with alternative approaches. For PACS detections, we compare in Figure 1 (top panel) our L_{IR} derived from SED fitting to the UV-PACS range with Polletta templates, with those computed by using the Chary & Elbaz (2001, hereafter CE01) library and fitting only the $100\mu\text{m}$ fluxes. This shows a very tight correspondence, confirming the value of far-IR information to constrain the bolometric energy budget of high- z galaxies, independently of the models assumed. For sources with $24\mu\text{m}$ detection and no PACS, we have to rely on large extrapolations, that can be strongly influenced by the adopted models. As an internal check, we then compare in Figure 1 (bottom panel) the IR luminosity derived from our UV-to- $24\mu\text{m}$ and the UV-to- $160\mu\text{m}$ SED fitting procedures. Different colors refer to various redshift intervals. As already discussed by Elbaz et al. 2010 and Nordon et al. 2010, at $z > 1.5$ L_{IR} based on $24\mu\text{m}$ data are overestimated, by a median factor ~ 1.8 in our analysis: this factor is larger for the CE01 models and when including PACS upper limits in the analysis (e.g. up to a factor ~ 4 , see Nordon et al. 2010, showing that the observed trend is not induced by any PACS incompleteness). At $z < 1.5$, the $24\mu\text{m}$ based L_{IR} are underestimated, up to a factor ~ 1.6 around $z \sim 0.5 - 1.0$. This result highlights

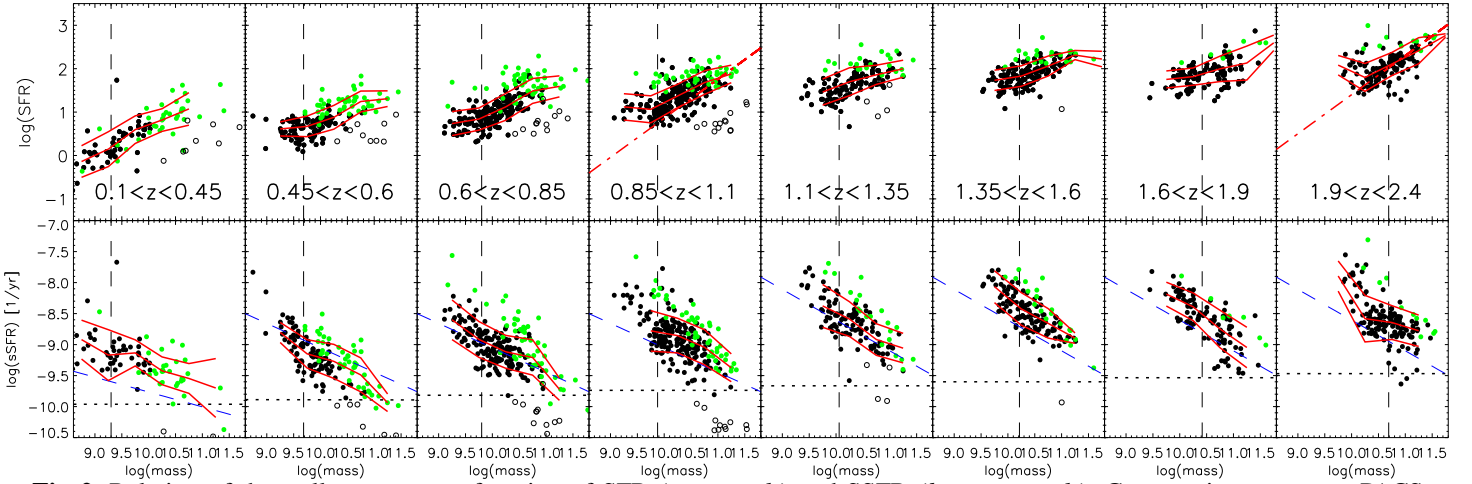


Fig. 2. Relation of the stellar mass as a function of SFR (*top panels*) and SSFR (*bottom panels*). Green points represent PACS detected sources for which the L_{IR} has been computed including all data points. Black points are MIPS $24\mu\text{m}$ sources undetected by PACS: in this case the L_{IR} has been derived from our SED fitting procedure limited at $24\mu\text{m}$. Open symbols are passive sources with color $\text{mag}[24]-\text{mag}[3.6]<0.5$. We also report with red lines the average of the relations and the $\pm 1\sigma$ limits. The red dot-dashed lines correspond to literature observed relations between mass and SFR: at $z \sim 1$ the GOODS relation by Elbaz et al. (2007); at $z \sim 2$ the relation for star-forming BzK by Daddi et al. (2007). Vertical dashed lines mark the mass completeness limit as a function of z , and the horizontal dotted lines indicate the inverse of the age of the universe at the mean redshift of each bin. The dashed blue lines in the bottom panels show the relations derived from our stacking analysis on PACS maps. Open circles mark sources classified as passive on a color basis ($\text{mag}[24]-\text{mag}[3.6]<0.5$), and generally populate a separate sequence (this bimodality has already been detected by Santini et al. 2009).

the key role of *Herschel* and have strong implications on previous *Spitzer* works on the SFR of $z \sim 2$ galaxies. In the following analysis and figures we have corrected the $24\mu\text{m}$ based L_{IR} , according to the new *Herschel* calibration that we have just discussed.

5.2. The mass versus SFR relation of star-forming galaxies

The existence of a strong correlation between galaxy SFR and mass at different redshifts ($0 < z < 3$) has been extensively discussed in the recent literature (Erb et al. 2006, Noeske et al. 2007a, Elbaz et al. 2007, Daddi et al. 2007, Perez-Gonzalez et al. 2008, Pannella et al. 2009, among the others), but there is not yet agreement on the general validity and properties of this relation. The main results of our analysis are shown in Figure 2 where we combine the subsamples of the *star-forming* galaxies detected with PACS and/or MIPS. The upper panels indicate the existence of a (rather scattered) positive correlations between the SFR and stellar mass at all redshifts. The Spearman test indicates that the probability of not having correlation is $2e-23$, $7e-23$, $9e-41$, $1e-28$, $2e-14$, $2e-17$, $4e-08$, and $1e-10$ in the eight redshift intervals, respectively. The SFR-mass relation looks more robust at $z < 1$. However we should remind that in this case we are considering also sources below the mass completeness (vertical lines), and that we are sampling only the most star-forming population, as MIPS or PACS undetected sources are not included in these plots. The comparison with Elbaz et al. (2007) at $z \sim 1$ and Daddi et al. (2007) at $z \sim 2$ (see caption of Figure 2 for details) shows that their observed slope of the SFR-mass relation is not inconsistent with our results, but even much flatter relations would be allowed by our data above the completeness limit. The lower panels of Figure 2 show the relation between SSFR and stellar mass for the same sources plotted in the upper panels. A negative trend of SSFR with mass is evident at all redshifts, although the scatter is quite large. The bulk of PACS and/or MIPS sources is located above the horizontal dotted line (the inverse of

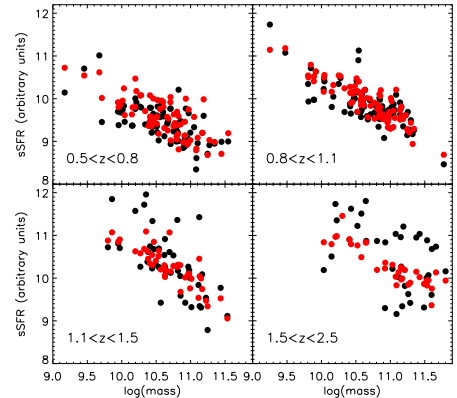


Fig. 3. Relation of the stellar mass as a function of the SSFR for PACS detected sources in various redshift bins: the SFR for red points has been computed from PACS fluxes, while for black points it has been extrapolated from the SED fitting from the $24\mu\text{m}$ data.

the age of the Universe), indicating that these systems are experiencing a major episode of star formation, forming stars more actively than in their recent past and building up a substantial fraction of their final stellar mass.

The key role of *Herschel* for high- z galaxies is highlighted in Figure 3 showing that when PACS data are used, the scatter of the SSFR - mass relations decreases by factors of 1.0, 1.3, 2.3 and 3.7 for increasing redshift bins, compared to the case of SSFRs estimated with MIPS data only. We have to warn that PACS detects only the brightest objects and we cannot then verify that the scatter is intrinsically lower. However, the fact that at least at high luminosities, at $z \sim 2$, PACS produces a smaller scatter (because it provides a more accurate SFR), might suggest that a similar trend should happen also at low luminosities.

6. Stacking analysis on PACS images

To test if the results in Figure 2 might have been affected by selection biases and to verify their reliability, we performed a stacking analysis (Bethermin et al. 2010) including all sources of the original IRAC [4.5]<23.0 sample. We splitted the sample in bins of mass and redshift, and stacked on a residual $160\mu\text{m}$ map (created by removing all PACS $160\mu\text{m}$ detections included in our catalog with $\text{SNR} > 3$) at the positions of all IRAC sources undetected by PACS (stacking at $100\mu\text{m}$ does not change our results). With this procedure, we derived a typical flux for each mass-redshift bin. Using the formalism introduced by Magnelli et al. (2009), that accounts both for detections and no-detections, we then converted these fluxes into luminosities by adopting an average K -correction for each redshift (derived from the more common SED template adopted by our best-fitting procedure in that interval). An empirical relation between rest-frame $\nu L_\nu(160\mu\text{m})$ and L_{IR} was used to first convert the stacked luminosities into bolometric luminosities, and then into SFR through a standard Kennicutt law (Kennicutt et al. 1998). In this analysis we have included only star-forming galaxies. To exclude passive sources we applied an empirical color selection of $(U - B)_{\text{rf}} < 1.1$, calibrated from our data, and, to recover massive dusty sources that might fall into the red sequence, we included in the stacking analysis also sources with $(U - B)_{\text{rf}} > 1.1$ and $\text{mag}[24] - \text{mag}[3.6] > 0.5$.

The results of the PACS stacking analysis are presented in Figure 4 (upper panel) and compared with literature data based on star-forming samples (with the exception of Dunne et al. 2009 that includes all K -band selected objects). The slope of our SSFR-mass relation becomes steeper with redshift, being quite flat at $z < 1$ with $\alpha = -0.25^{+0.11}_{-0.14}$ (all the slopes have been computed in a mass complete range). Intriguingly, the slopes are consistent with those observed for the 24, 100 and $160\mu\text{m}$ detections at $0.5 < z < 2$ (blue, long-dashed lines in Figure 3). At $z < 1$, our results are in broad agreement with those based on radio-stacking that found almost flat relations up to $z \sim 2$ (Dunne et al. 2009, Pannella et al. 2009), while at $z > 1$ our relation evolves toward stronger dependencies ($\alpha = -0.50^{+0.13}_{-0.16}$). We note that the rejection of passive and massive sources in the Dunne et al. sample would produce even flatter relations, increasing the discrepancy with our results at high- z . At low z , the study by Noeske et al. (2007) based on the UV-optical luminosities is steeper than our results, while at $z \sim 2$ the work by Erb et al. (2006) is more consistent with our observed SSFR-mass relation (however, within a very huge scatter). A recent work by Oliver et al. (2010), based on MIPS 70 and $160\mu\text{m}$ stacking, seems instead to be in general agreement with us up to $z < 1.5$, where they have enough statistics.

Figure 4 (bottom panel) also shows that the mean SSFR of star-forming sources rises with redshift, up to a factor ~ 15 for the most massive galaxies ($M > 10^{11} M_\odot$), implying that galaxies tend to form their stars more actively at higher redshifts. The mean SSFR seems also to flatten at $z > 1.5$ for ($M > 10^{10.5} M_\odot$). Moreover, the most massive galaxies have the lowest SSFR at any redshifts. As shown in bottom Fig.4, they have already so large stellar masses at $z=0.7$ to 2.5 that they would require steady SFR at the PACS observed level during the whole Hubble time at that redshift to form.

Acknowledgements. GR acknowledges support from the University of Padova from ASI (Herschel Science Contract I/005/07/0). PACS has been developed by a consortium of institutes led by MPE (Germany) and including UVIE (Austria); KU Leuven, CSL, IMEC (Belgium); CEA, LAM (France); MPIA (Germany); INAF-IFSI/OAA/OAP/OAT, LENS, SISSA (Italy); IAC (Spain). This development has been supported by the funding agencies BMVIT (Austria), ESA-

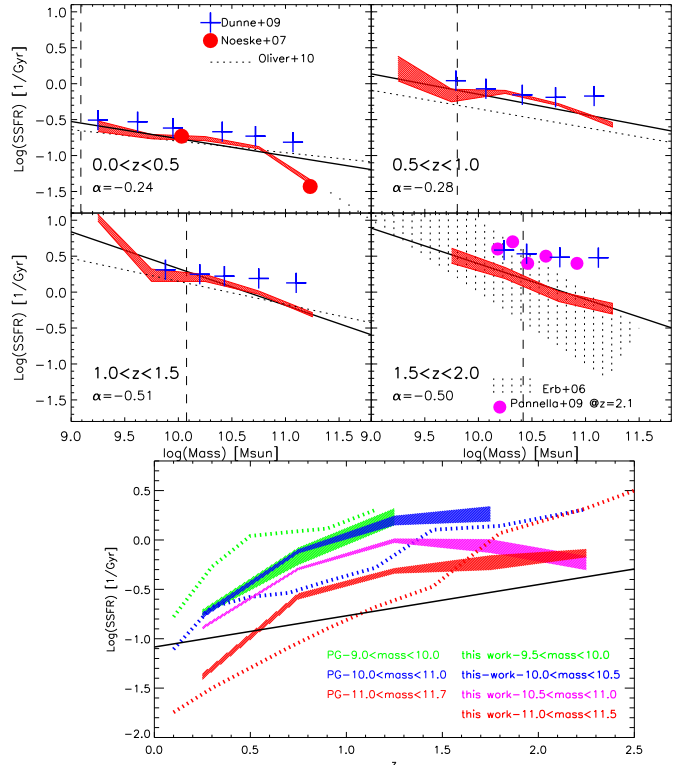


Fig. 4. Upper figure: SSFR-mass relation based on a stacking analysis on PACS images for a sample of IRAC $\text{mag}[4.5] < 23.0$ star-forming sources in various redshift bins. Our data are shown as a red shaded region, where the upper and lower envelopes of each curve represent the statistical errors derived from a bootstrapping procedure on the stacking analysis. The black solid lines mark linear fits to our distribution. Literature data are reported with different symbols (see legend in the Figure). Vertical lines mark the mass completeness. Lower figure: SSFR- z relation, in various mass bins. Our data (shaded regions) are compared to Perez-Gonzalez et al. (2008, dotted lines). The black line is the inverse of time since Bing Bang at any redshift.

PRODEX (Belgium), CEA/CNES (France), DLR (Germany), ASI/INAF (Italy), and CICYT/MCYT (Spain).

References

- Barger, A. J., Cowie, L. L., & Wang, W.-H. 2008, *ApJ*, 689, 687
 Berta et al., 2010 this volume
 Bethermin, M., Dole, H., Beelen, A., & Aussel, H. 2010, arXiv:1001.0896
 Bolzonella, M., Miralles, J.-M., & Pelló, R. 2000, *A&A*, 363, 476
 Bruzual, G., & Charlot, S. 2003, *MNRAS*, 344, 1000
 Chary, R., & Elbaz, D. 2001, *ApJ*, 556, 562
 Cowie, L. L., & Barger, A. J. 2008, *ApJ*, 686, 72
 Daddi, E., et al. 2007, *ApJ*, 670, 156
 da Cunha, E., Eminian, C., Charlot, S., & Blaizot, J. 2010, *MNRAS*, 273
 Damen, M., Labbé, I., Franx, M., et al. 2009, *ApJ*, 690, 937
 Dunne, L., et al. 2009, *MNRAS*, 394, 3
 Elbaz, D., et al. 2007, *A&A*, 468, 33
 Elbaz et al., 2010 this volume
 Erb, D. K., Steidel, C. C., Shapley, A. E., et al. 2006, *ApJ*, 647, 128
 Feulner, G., Gabasch, A., Salvato, M., et al. 2005, *ApJ*, 633, L9
 Gruppioni et al., 2010 this volume
 Kennicutt, R. C., Jr. 1998, *ApJ*, 498, 541
 Magnelli, B., Elbaz, D., Chary, R. R., et al. 2009, *A&A*, 496, 57
 Mancini, C., Matute, I., Cimatti et al. 2009, *A&A*, 500, 705
 Noeske, K. G., et al. 2007, *ApJ*, 660, L43
 Nordon et al., 2010 this volume
 Oliver, S., et al. 2010, arXiv:1003.2446
 Pannella, M., et al. 2009, *ApJ*, 698, L116
 Papovich, C., Rudnick, G., Le Floch, E. et al. 2007, *ApJ*, 668, 45

- Pérez-González, P. G., Trujillo, I., Barro, G., et al. 2008, ApJ, 687, 50
Pilbratt et al., 2010 this volume
Poglitsch et al., 2010 this volume
Polletta, M., et al. 2007, ApJ, 663, 81
Rodighiero, G., Cimatti, A., Franceschini, A. et al. M. 2007, A&A, 470, 21
Rodighiero, G., et al. 2010 A&A preprint doi
<http://dx.doi.org/10.1051/0004-6361/200912058>
Santini, P., et al. 2009, A&A, 504, 751

Appendix A: Authors affiliations

- ¹ Department of Astronomy, University of Padova, Vicolo dell'Osservatorio 3, I-35122 Padova, Italy. e-mail: giulia.rodighiero@unipd.it
- ² Dipartimento di Astronomia, Università di Bologna, via Ranzani 1, I-40127 Bologna, Italy
- ³ INAF-Osservatorio Astronomico di Bologna, Via Ranzani 1, I-40127, Bologna, Italy
- ⁴ Max-Planck-Institut für extraterrestrische Physik, Postfach 1312, 85741 Garching, Germany
- ⁵ European Southern Observatory, Karl-Schwarzschild-Str. 2, 85748 Garching, Germany
- ⁶ INAF-Osservatorio Astronomico di Roma, via di Frascati 33, 00040 Monte Porzio Catone, Italy.
- ⁷ ESAC, Villafranca del Castillo, ES-28691 Madrid, Spain
- ⁸ Laboratoire AIM, CEA/DSM-CNRS-Université Paris Diderot, IRFU/Service d'Astrophysique, Bât.709, CEA-Saclay, 91191 Gif-sur-Yvette Cedex, France.
- ⁹ Instituto de Astrofísica de Canarias, 38205 La Laguna, Spain.
- ¹⁰ Department of Astronomy, 610 Space Sciences Building, Cornell University, Ithaca, NY 14853, USA
- ¹¹ INAF-IFSI, Via Fosso del Cavaliere 100, I-00133 Roma, Italy
- ¹² INAF-Osservatorio Astronomico di Padova, Vicolo dell'Osservatorio 2, I-35122 Padova, Italy
- ¹³ INAF-Osservatorio Astronomico di Trieste, via Tiepolo 11, 34143 Trieste, Italy

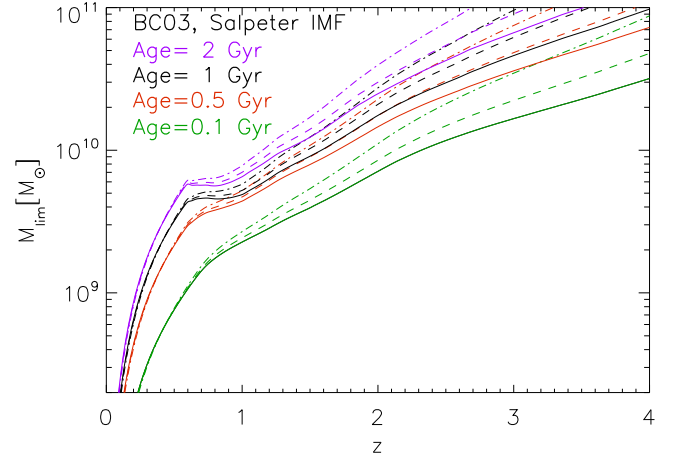
Appendix B: Mass completeness**Appendix C: SED fitting examples**

Fig. B.1. Mass-completeness thresholds as a function of redshift for our IRAC $4.5\mu\text{m}$ -selected sample ($\text{mag}_{4.5\mu\text{m}} < 23.0$, AB), derived from synthetic stellar population models as described in Mancini et al. (2009). Here we used the constant SFR templates of Bruzual & Charlot (2003), with a Salpeter IMF, and different ages, and dust extinction parameters (E_{B-V}). For each specific age, we considered three possible values of dust extinction: $E_{B-V} = 0.3$ (solid lines), $E_{B-V} = 0.5$ (dashed lines), and $E_{B-V} = 0.8$ (dot-dashed lines). In our analysis we adopted the most conservative mass-completeness limit (dot-dashed magenta line), above which even the oldest (2 Gyr) and highly extinguished ($E_{B-V} = 0.8$) star-forming galaxy population would be entirely recovered.

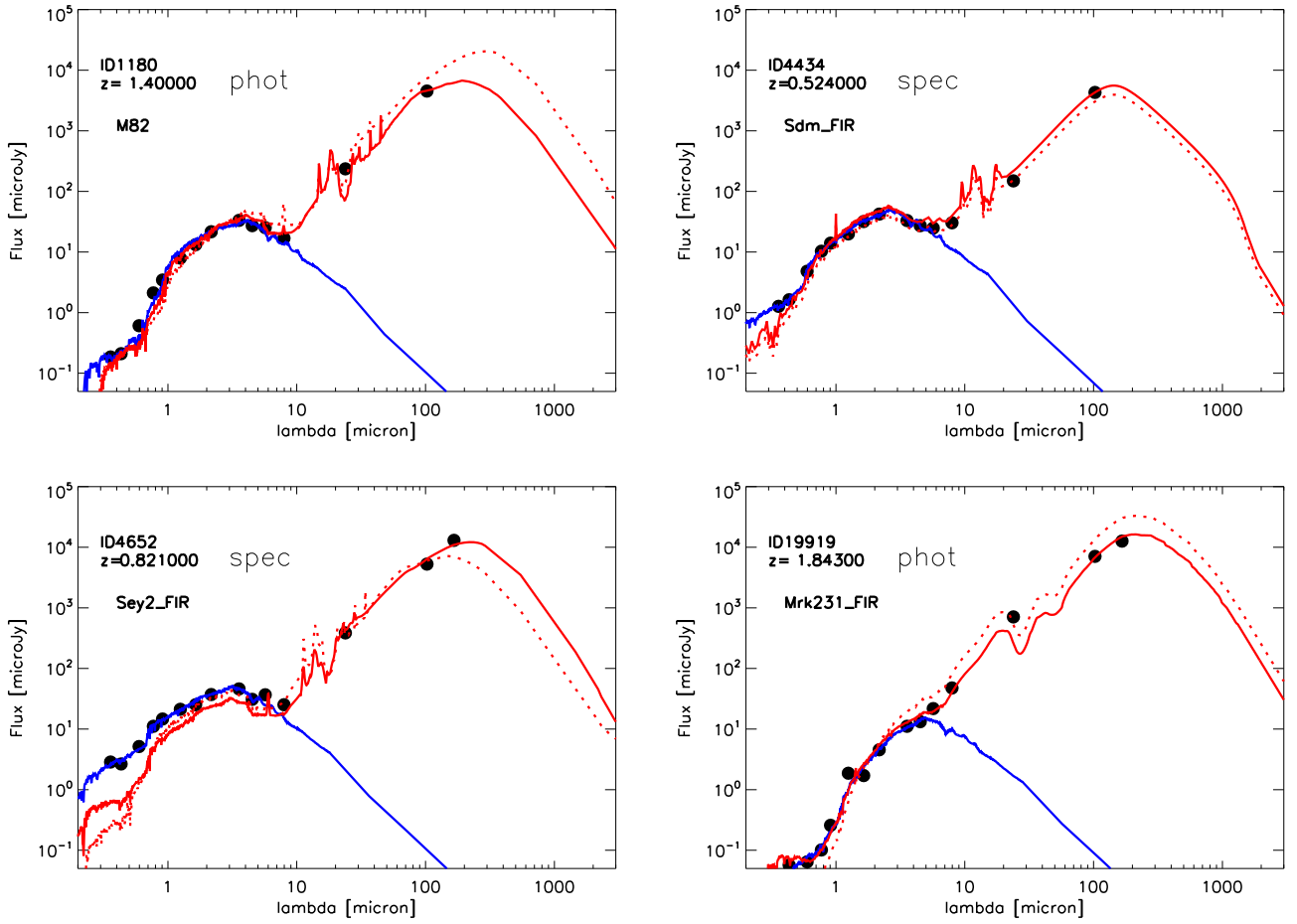


Fig. C.1. The observed Spectral Energy Distributions (filled circles) of four PACS sources from our sample, representative of the various spectral classes considered in this work. We also show the best-fit spectra obtained with *Hyperz* based on the spectral library by Polletta et al. (2007) and the updated version of Gruppioni et al. (2010): the red solid lines represent the best-fit obtained with *Herschel* data, while red dotted lines are the fit limited to the $24\mu\text{m}$ *Spitzer* data points. The blue lines show the fit to the optical- $5.8\mu\text{m}$ bands with Bruzual & Charlot (2003) models .